J|A|C|S ARTICLES

Published on Web 03/15/2010

# Impacts of Mesoporous Silica Nanoparticle Size, Pore Ordering, and Pore Integrity on Hemolytic Activity

Yu-Shen Lin and Christy L. Haynes*

*Department of Chemistry, University of Minnesota, 207 Pleasant Street SE, Minneapolis, Minnesota 55455*

Received December 23, 2009; E-mail: chaynes@umn.edu

***Abstract:*** This paper uses the measure of hemolysis to evaluate the toxicity of nonporous and porous silica nanoparticles with varied sizes and investigates the effects of porous structure and integrity on the nanoparticle−cell interaction. The results show that both nonporous and porous silica cause red blood cell membrane damage in a concentration- and size-dependent manner. In the case of mesoporous silica nanoparticles, the size-dependent hemolysis effect is only present when the nanoparticles have long-range ordered porous structure, revealing that pore structure is critical in cell−nanoparticle interactions. Mesoporous silica nanoparticles show lower hemolytic activity than their nonporous counterparts of similar size, likely due to fewer silanol groups on the cell-contactable surface of the porous silica nanoparticles. The extent of hemolysis by mesoporous silica nanoparticles increases as the pore structure is compromised by mild aging in phosphate-buffered solutions, initiating mesopore collapse. The pore integrity of mesoporous silica nanoparticles is examined by TEM, XRD, $N_2$ adsorption−desorption isotherms, and quantification of dissolved silica. In these nanoparticles, pore stability is clearly an important factor in determining the hemolytic activity; further work demonstrates that nanoparticle-induced hemolysis can be eliminated by modifying the silanol surface with a poly(ethylene glycol) coating.

## Introduction

Humans are exposed to silica, the most abundant substance in nature, extensively in our daily life from sources as ubiquitous as rocks, sand, and clays. Industrial silica products, such as fumed silica and silica gel, are widely used in the electronics industry and as a food additive.[1] With the rapid advance of nanoscience over the past decades, nanosized nonporous amorphous silica has been investigated intensively and used in a wide variety of applications including catalytic supports,[2] photonic crystals,[3] gene delivery,[4] photodynamic therapy,[5] and biomedical imaging.[6] Based on mature silica condensation chemistry, surfactant-templating methods can be easily applied to create amorphous mesoporous silica nanomaterials as well. These mesoporous nanoparticles have recently attracted much attention in the biomedical field due to their unique characteristics, including a large internal surface area and volume, making them excellent candidates for stealth drug delivery (assuming that their unintentional toxicity is minimal). Accordingly, much research effort has focused on developing multifunctional mesoporous nanoparticles for in vivo tumor imaging,[7] labeling,[8] and therapeutic use;[9,10] it is clear that any potential cytotoxic effects of these nanoparticles should be evaluated as the materials evolve to inform continued fabrication efforts. However, compared to the many published reports investigating the in vitro and in vivo cytotoxicity of nonporous silica nanoparticles,[11−16] there are very few studies systematically investigating the toxicity of mesoporous silica nanoparticles either in vitro or in vivo.[17−20] Vallhov and co-workers studied the size effect of mesoporous silica particles (with diameters of 270 nm and 2.5 $\mu$m) on the immune response of human monocyte-

(1) Barik, T. K.; Sahu, B.; Swain, V. *Pediatr. Res.* **2008**, *103*, 253–258.
(2) Kim, J.; Lee, J. E.; Lee, J.; Jang, Y.; Kim, S.-W.; An, K.; Yu, J. H.; Hyeon, T. *Angew. Chem., Int. Ed.* **2006**, *45*, 4789–4793.
(3) Lin, Y.-S.; Hung, Y.; Lin, H.-Y.; Tseng, Y.-H.; Chen, Y.-F.; Mou, C.-Y. *Adv. Mater.* **2007**, *19*, 577–580.
(4) Roy, I.; Ohulchanskyy, T. Y.; Bharali, D. J.; Pudavar, H. E.; Mistretta, R. A.; Kaur, N.; Prasad, P. N. *Proc. Natl. Acad. Sci. U.S.A.* **2005**, *102*, 279–284.
(5) Ohulchanskyy, T. Y.; Roy, I.; Goswami, L. N.; Chen, Y.; Bergey, E. J.; Pandey, R. K.; Oseroff, A. R.; Prasad, P. N. *Nano Lett.* **2007**, *7*, 2835–2842.
(6) Lu, C.-W.; Hung, Y.; Hsiao, J.-K.; Yao, M.; Chung, T.-H.; Lin, Y.-S.; Wu, S.-H.; Hsu, S.-C.; Liu, H.-M.; Mou, C.-Y.; Yang, C.-S.; Huang, D.-M.; Chen, Y.-C. *Nano Lett.* **2007**, *7*, 149–154.
(7) Lee, J. E.; Lee, N.; Kim, H.; Kim, J.; Choi, S. H.; Kim, J. H.; Kim, T.; Song, I. C.; Park, S. P.; Moon, W. K.; Hyeon, T. *J. Am. Chem. Soc.* **2010**, *132*, 552–557.
(8) Liong, M.; Lu, J.; Michael, K.; Xia, T.; Ruehm, S. G.; Nel, A. E.; Tamanoi, F.; Zink, J. I. *ACS Nano* **2008**, *2*, 889–896.
(9) Tu, H.-L.; Lin, Y.-S.; Lin, H.-Y.; Hung, Y.; Lo, L.-W.; Chen, Y.-F.; Mou, C.-Y. *Adv. Mater.* **2009**, *21*, 172–177.
(10) Zhao, Y.; Trewyn, B. G.; Slowing, I. I.; Lin, V. S.-Y. *J. Am. Chem. Soc.* **2009**, *131*, 8398–8400.
(11) Lin, W.; Huang, Y.-w.; Zhou, X.-D.; Ma, Y. *Toxicol. Appl. Pharmacol.* **2006**, *217*, 252–259.
(12) Chang, J.-S.; Chang, K. L. B.; Hwang, D.-F.; Kong, Z.-L. *Environ. Sci. Technol.* **2007**, *41*, 2064–2068.
(13) Yu, K. O.; Grabinski, C. M.; Schrand, A. M.; Murdock, R. C.; Wang, W.; Gu, B.; Schlager, J. J.; Hussain, S. M. *J. Nanopart. Res.* **2009**, *11*, 15–24.
(14) Napierska, D.; Thomassen, L. C. J.; Raboli, V.; Lison, D.; Gonzalez, L.; Kirsch-Volders, M.; Martens, J. A.; Hoet, P. H. *Small* **2009**, *5*, 846–853.
(15) Kaewamatawong, T.; Kawamura, N.; Okajima, M.; Sawada, M.; Morita, T.; Shimada, A. *Toxicol. Pathol.* **2005**, *33*, 745–751.
(16) Cho, W.-S.; Choi, M.; Han, B. S.; Cho, M.; Oh, J.; Park, K.; Kim, S. J.; Kim, S. H.; Jeong, J. *Toxicol. Lett.* **2007**, *175*, 24–33.
(17) Vallhov, H.; Gabrielsson, S.; Strømme, M.; Scheynius, A.; Garcia-Bennett, A. E. *Nano Lett.* **2007**, *7*, 3576–3582.

 **10.1021/ja910846q** 

drived dendritic cells (MDDCs) and concluded that smaller particles had lower cytotoxicity to MDDCs.[17] In contrast, recent work reported by Kohane and co-workers compared the cytotoxicity of spherical mesoporous silica particles having three different diameters (190 nm, 420 nm, and 1.22 $\mu$m) and concluded that the smaller particles show higher cytotoxicity on human breast cancer cells.[20] Clearly, there is disagreement about the size-dependent cytotoxicity of mesoporous silica nanoparticles, but a more critical issue is that there is no size-dependent toxicity study of mesoporous silica in the size regime relevant for injectable drug delivery nanoparticles. For this application, the nanoparticle must be less than 100 nm diameter in order to avoid immediate uptake by the reticuloendothelial system (RES),[21] a process which removes the nanoparticle from circulation and eliminates the opportunity to deliver the loaded drug.

Because it has been possible to prepare nonporous silica particles with varied sizes for many years, nonporous silica particles have been employed in cytotoxicity studies investigating the effect of nanoparticle size. Multiple research groups have shown that ultrafine amorphous nonporous silica nanoparticles (<50 nm diameter) reduce in vitro cell viability[13,14] and cause more severe in vivo lung inflammation than that caused by fine silica particles (>200 nm diameter).[15] In the case of mesoporous silica toxicity studies, however, only nanoparticles with diameters greater than 100 nm have been investigated either in vitro or in vivo, largely due to difficulties in fabricating uniform mesoporous nanoparticles with smaller diameters.[17−19] Recently, several groups have demonstrated fabrication schemes to achieve smaller mesoporous silica nanoparticle diameters in hopes of minimizing nanoparticle uptake by the RES when the biomedical porous nanoparticles are administrated intravenously.[22−24] With these recent advances, not only have mesoporous silica nanoparticles become a more plausible biomedical device but it is finally possible to evaluate the size effects on mesoporous silica nanoparticle toxicity in a relevant size regime. In addition, up to now, none of the reported papers investigate the effect of pore structure and pore stability on mesoporous silica hemolytic activity. Herein, we demonstrate how mesoporous nanoparticle size, pore structure, and pore stability influence cytotoxicity as compared to their nonporous counterparts with analogous size.

Characterization of in vitro blood compatibility of the porous nanoparticles is especially important because biomedical applications require the nanoparticles to be delivered via intravenous injection. To date, only two papers compare the in vitro hemolytic activity between nonporous and porous silica particles.[24,25] Slowing et al. reported that large mesoporous silica particles (100−300 nm diameter) showed low hemolytic activity in red blood cells (RBCs) compared to commercial silica particles and that the hemolysis of RBCs is strongly related to the number of silanol groups on the surface of the nanoparticles.[25] In the second report, our own previous work, it was clear that mesoporous silica-coated multifunctional nanoparticles exhibited lower hemolytic activity than nonporous silica-coated nanoparticles.[24] Neither of these reports, however, systematically investigates nanoparticle size, pore structure, and pore stability effects on the hemolytic capacity of mesoporous silica nanoparticles even though these characteristics are critical in determining the nanoparticles' utility for their intended application as a therapeutic.

In this work, nonporous Stöber and mesoporous silica nanoparticles with varied sizes ranging from ∼25 to ∼250 nm diameter were prepared. A simple hemolysis assay is employed to assess and compare the human red blood cell compatibility of these nonporous and porous silica nanoparticles. Hemolysis is also monitored following cell exposure to nanoparticles with varied pore structure, stability, and surface modification, revealing the critical design parameters to achieve silica nanomaterials with minimal biological impact. This is the first work that systematically studies the influence of mesoporous silica nanoparticle size (within a drug delivery-relevant regime), pore structure, and pore stability on hemolytic activity.

## Experimental Section

**Chemicals.** All chemicals were used without additional purification. *n*-Cetyltrimethylammonium bromide (CTAB, 99%) and tetraethyl orthosilicate (TEOS, 98%) were purchased from Sigma Aldrich (Milwaukee, WI). [Hydroxy(polyethyleneoxy)propyl-]triethoxysilane (PEG-silane, MW 575−750 g/mol, 8−12 EO, 50% in ethanol) was obtained from Gelest (Morrisville, PA). Ammonium nitrate (99.9%) and ammonium hydroxide ($NH_4OH$, 28−30 wt % as $NH_3$) were obtained from Mallinckrodt (Phillipsburg, NJ). Absolute anhydrous ethanol and 95% ethanol were purchased from Pharmco-Aaper (Brookfield, CT). Calcium- and magnesium-free Dulbecco's phosphate-buffered saline (PBS) was obtained from Invitrogen (Grand Island, NY). The deionized (D.I.) water was generated using a Millipore Milli-Q system (Billerica, MA).

**Characterization.** Transmission electron microscopy (TEM) micrographs were taken on a JEOL 1200 EXII (Tokyo, Japan) with a 100 kV voltage. TEM specimens were prepared by evaporating one drop of ethanolic nanoparticle solution on Ted Pella Formvar-coated copper grids (Redding, CA). Nanoparticle size was measured in the micrographs using Sigma Scan Pro 5.0 software (Ashburn, VA). Powder XRD data were recorded on a Siemens Bruker-AXS D-5005 X-ray diffractometer using filtered Cu K$\alpha$ radiation ($\lambda$ = 1.5406 Å) at 45 kV and 20 mA. Data were recorded by step scan with a step size of 0.040° and a step time of 1.0 s. Nitrogen adsorption−desorption measurements were carried out on a Quantachrom Autosorb-1 analyzer (Boynton Beach, FL) at 77 K. Samples were outgassed at 120 °C for at least 12 h before measurements. The specific surface area was calculated using Brunauer−Emmett−Teller (BET) equation at $P/P_0$ <0.3. The pore size distribution was calculated from the branch of the adsorption isotherm using a Barrett−Joyner−Halenda (BJH) method. The primary and total pore volume was determined at $P/P_0 = 0.50$ and 0.99, respectively. The absorbance of hemoglobin was measured using a Bio-Rad iMark microplate reader (Hercules, CA).

**Preparation of Nonporous and Porous Silica Nanoparticles (NPs). a. Synthesis of Stöber Silica (SS) NPs with Varied Sizes.** Uniform nonporous silica nanospheres were synthesized using a well-known method developed by Stöber et al.[26] The nonporous silica particle diameter was tuned by varying the amounts of ammonium hydroxide and TEOS. The synthesis conditions and

(18) Di Paqua, A. J.; Sharma, K. K.; Shi, Y.-L.; Toms, B. B.; Ouellette, W.; Dabrowiak, J. C.; Asefa, T. *J. Inorg. Biochem.* **2008**, *102*, 1416–1423.
(19) Hudson, S. P.; Padera, R. F.; Langer, R.; Kohane, D. S. *Biomaterials* **2008**, *29*, 4045–4055.
(20) He, Q.; Zhang, Z.; Gao, Y.; Shi, J.; Li, Y. *Small* **2009**, *5*, 2722–2729.
(21) He, X.; Nie, H.; Wang, K.; Tan, W.; Wu, X.; Zhang, P. *Anal. Chem.* **2008**, *80*, 9597–9603.
(22) Kim, J.; Kim, H. S.; Lee, N.; Kim, T.; Kim, H.; Yu, T.; Song, I. C.; Moon, W. K.; Hyeon, T. *Angew. Chem., Int. Ed.* **2008**, *47*, 8438–8441.
(23) Lu, F.; Wu, S.-H.; Hung, Y.; Mou, C.-Y. *Small* **2009**, *5*, 1408–1413.
(24) Lin, Y.-S.; Haynes, C. L. *Chem. Mater.* **2009**, *21*, 3979–3986.
(25) Slowing, I. I.; Wu, C.-W.; Vivero-Escoto, J. L.; Lin, V. S.-Y. *Small* **2009**, *5*, 57–62.
(26) Stöber, W.; Fink, A.; Bohn, E. *J. Colloid Interface Sci.* **1968**, *26*, 62–69.

composition of the synthesis mixture are described in Table S1 (in the Supporting Information). The as-synthesized SS NPs were collected by centrifugation and washed with absolute ethanol twice to remove unreacted precursors. All SS NPs for hemolysis assays were suspended and diluted in PBS before use. The SS NPs with mean diameters of 24, 37, 142, and 263 nm are referred to as SS-24, SS-37, SS-142, and SS-263, respectively.

**b. Synthesis of Mesoporous Silica (MS) and Poly(ethylene glycol) (PEG)-Coated MS NPs with Varied Sizes.** The porous silica NPs were prepared using an ammonia base-catalyzed method under highly dilute and low surfactant conditions.[27] The particle size was controlled by adjusting ammonia concentration,[23] TEOS volume added, and reaction temperature. The detailed synthesis conditions are shown in Table S2 (in the Supporting Information). Typically, 0.29 g of CTAB was dissolved in 150 mL of ammonium hydroxide solution (0.128, 0.256, 0.512, 0.768, and 1.024 M) at the desired temperature (30, 40, 50, 60 °C). Then, 0.88 M ethanolic TEOS was added to the solution under vigorous stirring (600 rpm). After 1 h, the mixture solution was aged for at least 12 h in static conditions. The as-synthesized colloid was transferred to 50 mL of ethanolic ammonium nitrate solution (6 g/L) with continual stirring at 60 °C for 1 h to remove surfactant. The surfactant extraction step was repeated two times to ensure removal of CTAB. The extracted NPs were washed with ethanol twice and resuspended in absolute ethanol. All MS NPs were suspended and diluted in PBS before hemolysis assay use. The MS NPs with mean diameters of 25, 42, 93, 155, and 225 nm are designated as MS-25, MS-42, MS-93, MS-155, and MS-225, respectively. To modify the outer surface of MS NPs, 600 $\mu$L of PEG-silane (50% in ethanol) was added after the formation of MS NPs. Herein, two sizes of MS NPs, MS-25 and MS-42, were chosen as PEG-modified examples. The code names for PEG-modified MS NPs were MS-25@PEG and MS-42@PEG, respectively.

**Assessing the Pore Stability of MS-25, MS-42, MS-25@PEG, and MS-42@PEG.** All stability test samples were prepared in PBS solution at 2 mg/mL concentration and aged for 6 days at room temperature. Then, the aged NPs were centrifuged, and the supernatant was saved for hemolysis assays. The obtained NPs were washed with absolute ethanol two times and dried at 60 °C. The solid products were used for XRD and $N_2$ adsorption−desorption characterization.

**Hemolysis Assay.** Ethylenediamine tetraacetic acid (EDTA)-stabilized human blood samples were freshly obtained from Memorial Blood Center (St. Paul, MN). First, 5 mL of blood sample was added to 10 mL of PBS, and then red blood cells (RBCs) were isolated from serum by centrifugation at 10016*g* for 10 min. The RBCs were further washed five times with 10 mL of PBS solution. The purified blood was diluted to 50 mL of PBS. Prior to nanoparticle exposure, the absorbance spectrum of the positive control supernatant was checked and used only if it was in the range of 0.50−0.55 optical density units to reduce sample difference from different donors. Herein, RBC incubation with D.I. water and PBS were used as the positive and negative controls, respectively. Then 0.2 mL of diluted RBC suspension was added to 0.8 mL of Stöber and mesoporous silica nanoparticle solutions at systematically varied concentrations and mixed by vortexing. The silica NPs suspended in PBS solutions with different concentrations were prepared immediately before red blood cell incubation by serial dilution. All the sample tubes were kept in static condition at room temperature for 3 h. Finally, the mixtures were centrifuged at 10016*g* for 3 min, and 100 $\mu$L of supernatant of all samples was transferred to a 96-well plate. The absorbance values of the supernatants at 570 nm were determined by using a microplate reader with absorbance at 655 nm as a reference. The percent hemolysis of RBCs was calculated using the following formula: percent hemolysis = ((sample absorbance − negative control absorbance)/(positive control absorbance − negative control absorbance)) × 100.

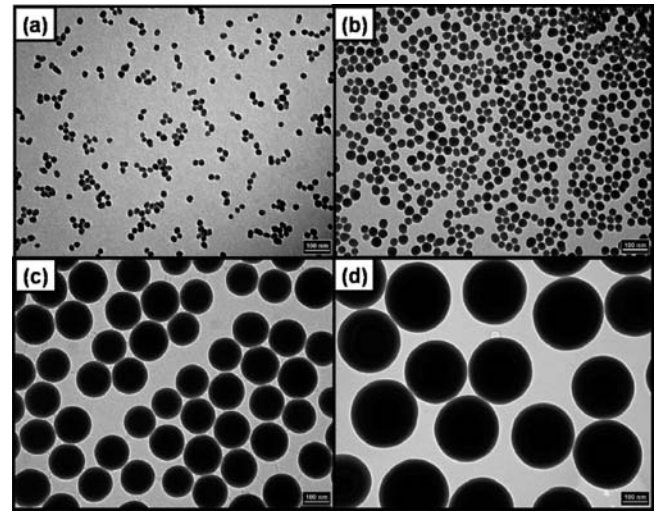


***Figure 1.*** TEM images of SS NPs with varied diameters: (a) SS-24, (b) SS-37, (c) SS-142, and (d) SS-263.

**Calculations and Data Analysis.** Every experimental condition was repeated at least three times in triplicate. All hemolysis data are presented as mean ± standard deviation (SD). The concentration leading to 50% lysis of RBCs ($TC_{50}$) was determined using ED50plus v1.0 software.[14] The statistical significance of the data was analyzed using the unpaired and two-tailed Student's *t* test (Prism, GraphPad software, San Diego, CA). When $p < 0.05$, the differences between data sets was considered to be statistically significant. The detailed calculations of NP number density per gram of SS and MS NPs are described explicitly in the Supporting Information.

## Results and Discussion

**Preparation and Characterization of SS and MS NPs.** In this study, two types of amorphous silica particles, nonoporous and porous NPs, were used to investigate the influence of nanoparticle size on hemolytic activity. The monodisperse nonporous silica NPs were prepared using the common base-catalyzed Stöber preparation. Typical TEM images in Figure 1 show the SS NPs having four distinct diameters. The size of SS NPs increases as the amount of TEOS and ammonium hydroxide used in the synthetic procedure are increased. On the basis of TEM images, the average diameter of these SS NPs is 24 ± 2.9, 37 ± 4.5, 142 ± 12, and 263 ± 14 nm, respectively (Figure S1 of the Supporting Information). The surface area of the SS NPs with varied sizes was determined by measuring $N_2$ adsorption−desorption isotherms and application of BET modeling. All the isotherms from SS NPs showed a typical type II isotherm that is characteristic of nonporous silica (one example shown in Figure S3 of Supporting Information).[28] The BET surface area data shows that the external surface area per gram of SS NPs decreases as the size increases, as listed in Table 2.

The porous silica NPs were synthesized by using a positively charged CTAB-template and $NH_4OH$ catalyst under dilute aqueous conditions. A photograph of the as-synthesized MS colloidal aqueous solutions shows that solution appearance changes from clear to turbid as the size of NPs increases (Figure S2 of Supporting Information). The Tyndall effect can be seen

(27) Lin, Y.-S.; Tsai, C.-P.; Huang, H.-Y.; Kuo, C.-T.; Hung, Y.; Huang, D.-M.; Chen, Y.-C.; Mou, C.-Y. *Chem. Mater.* **2005**, *17*, 4570–4573.

(28) Sing, K. S. W.; Everett, D. H.; Haul, R. A. W.; Moscou, L.; Pierotti, R. A.; Rouquérol; Siemieniewska, T. *Pure Appl. Chem.* **1985**, *57*, 603–619.

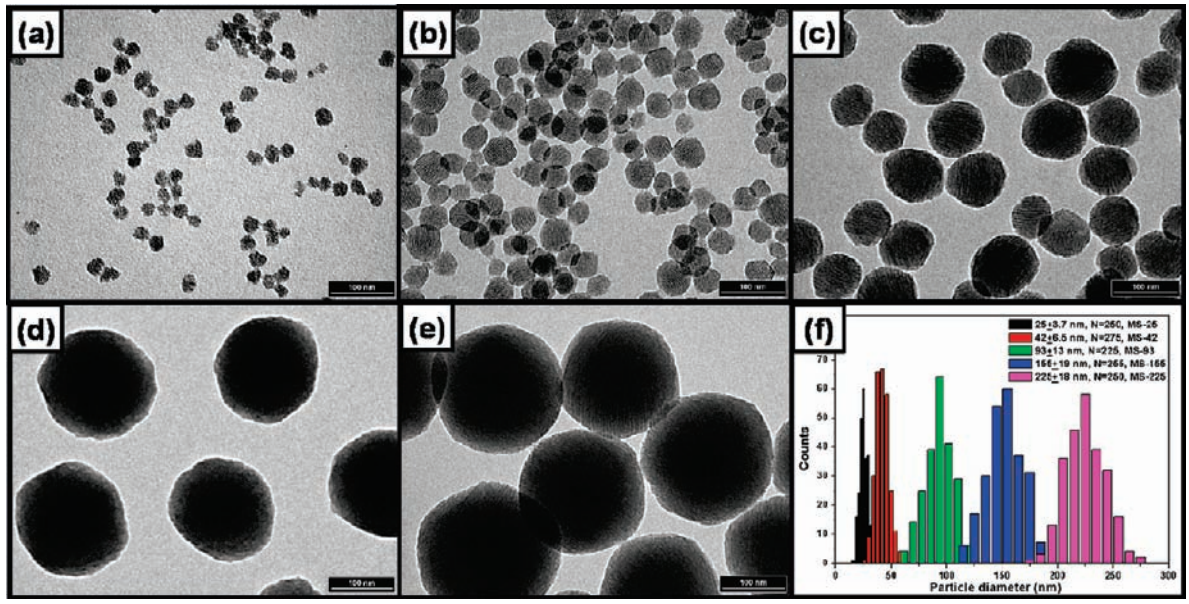


***Figure 2.*** TEM images of surfactant-free MS NPs with varied sizes: (a) MS-25, (b) MS-42, (c) MS-93, (d) MS-155, and (e) MS-225. (f) Particle size distributions of five sizes of surfactant-free MS NPs. The data were from TEM micrographs.

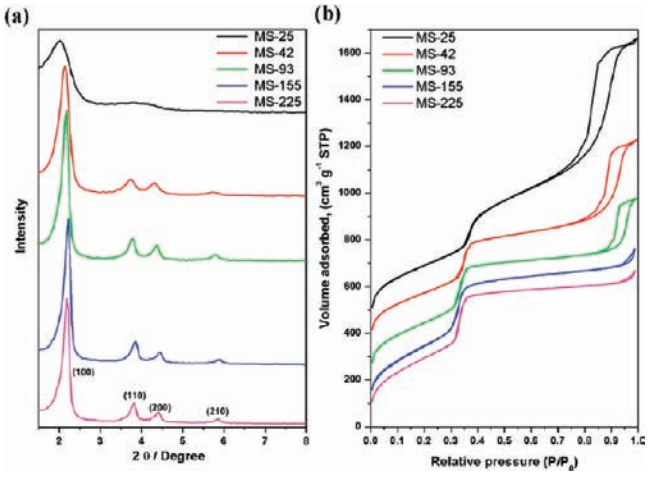


***Figure 3.*** Characterization of surfactant-free MS NPs. (a) Low-angle (1.5−8°) XRD patterns of MS NPs with varied sizes. (b) $N_2$ adsorption−desorption isotherms of MS NPs with varied sizes.

clearly when light passes through the transparent colloidal solution formed from 25-nm-diameter mesoporous silica nanoparticles. The TEM images and size distribution histograms in Figure 2 show the surfactant-free MS NPs with average sizes of 25 ± 3.7, 42 ± 6.5, 93 ± 13, 155 ± 19, and 225 ± 18 nm, respectively. The size of MS NPs increases as the NP synthesis incorporates higher ammonia concentration, more silica precursor, and lower temperature conditions. The pore structure of all five MS NP sizes was examined using low-angle powder XRD (Figure 3a). For the four largest diameter NPs, MS-42, MS-93, MS-155, and MS-225, four characteristic XRD peaks, (100), (110), (200), and (210), are present which indicate two-dimensional (2D) long-range ordering and a hexagonal pore structure. The XRD pattern of the smallest porous nanoparticle, MS-25, shows two broad peaks which suggest short-range ordering and a wormlike pore structure inside the NPs. This result can be confirmed visually in TEM images of MS-25 (Figure 2a). All of the $N_2$ adsorption−desorption isotherms in Figure 3b exhibit a steep adsorption behavior at $P/P_0$ around 0.35 without a hysteresis loop, known as a type IV isotherm according to IUPAC classification.[28] To further compare the structural properties of the MS NPs with varied sizes, the interplanar spacing, unit cell, surface area, pore size, and pore volume data from XRD and $N_2$ sorption measurements are summarized in Table 1. The $d_{100}$ spacing, BJH pore size, and primary pore volume of all MS samples with long-range ordered structure is around 4.05 nm, 2.50 nm, and 0.85 $cm^3\ g^{-1}$, respectively. Compared to well-ordered MS NPs, the MS-25 NPs have greater *d* spacing and pore size. In addition, the total pore volume of MS NPs per gram increases as the NP diameter decreases. The second adsorption of the isotherms at high relative pressure ($P/P_0 > 0.8$) represents the formation of interstitial pores among the dried NP agglomerates called textural porosity. The textural pore volume of MS NPs increases as the NP size decreases because more interstitial pores are formed between the smaller NPs. All the MS NPs have high total surface area ranging from 1038 to 1164 $m^2/g$. One important thing to keep in mind is that the obtained total surface area includes both internal and external surface area. Quantitative external surface areas of the MS NPs with varied diameter are difficult to determine from the total surface area data.

**Dose- and Size-Dependent Hemolytic Activity of SS and MS NPs.** The hemolysis assay was used to evaluate the cytotoxic effect of nonporous and porous silica NPs on human RBCs because silica materials have been known to cause membrane damage to RBCs.[29,30] To determine the concentration leading to 50% lysis of RBCs ($TC_{50}$) of each nanoparticle, the RBCs were exposed to each NP sample at a range of concentrations from 3.125 to 1600 $\mu$g/mL for 3 h. The highest doses used in this work were chosen to model doses often used for in vivo biodistribution, imaging, and therapeutic experiments. As shown in Figure 4a, the hemolysis percentage of RBCs increases in a dose-dependent manner. The photographs of RBCs after exposure to four diameters of SS NPs for 3 h are shown in Figure

(29) Gerashchenko, B. I.; Gun'ko, V. M.; Gerashchenko, I. I.; Mironyuk, I. F.; Leboda, R.; Hosoya, H. *Cytometry* **2002**, *49*, 56–61.
(30) Murashov, V.; Harper, M.; Demchuk, E. *J. Occup. Environ. Hygiene* **2006**, *3*, 718–723.

**Table 1.** Structural Properties of Surfactant-Free MS NPs with Varied Sizes

| samples | $d_{100}$[a] (nm) | $a$[b] (nm) | $S_{BET}$[c] ($m^2g^{-1}$) | $D_{BJH}$[d] (nm) | $V_t$[e] ($cm^3g^{-1}$) | $V_p$[f] ($cm^3g^{-1}$) | $V_{text}$[g] ($cm^3g^{-1}$) |
|---|---|---|---|---|---|---|---|
| MS-25 | 4.46 | 5.15 | 1164 | 2.74 | 2.00 | 0.92 | 1.08 |
| MS-42 | 4.13 | 4.77 | 1038 | 2.59 | 1.41 | 0.81 | 0.60 |
| MS-93 | 4.05 | 4.67 | 1089 | 2.51 | 1.28 | 0.86 | 0.42 |
| MS-155 | 4.05 | 4.67 | 1105 | 2.40 | 1.09 | 0.88 | 0.21 |
| MS-225 | 4.05 | 4.67 | 1123 | 2.41 | 1.04 | 0.89 | 0.15 |
| MS-25 after 6-day PBS aging | 4.46 | 5.15 | 738 | | 2.23 | 0.47 | 1.76 |
| MS-42 after 6-day PBS aging | 3.98 | 4.60 | 791 | | 1.89 | 0.51 | 1.38 |

[a] $d_{100}$, (100) interplanar spacing. [b] $a$, unit cell length of hexagonal packing structure. [c] $S_{BET}$: specific surface area calculated from data in the range $P/P_0 < 0.3$ using BET equation; [d] $D_{BJH}$: pore diameter assigned from the maximum on the BJH pore size distribution. [e] $V_t$: total pore volume calculated at $P/P_0 = 0.99$. [f] $V_p$: primary pore volume obtained from $P/P_0 = 0.50$. [g] $V_{text}$: textural pore volume was calculated using $V_t - V_p$.

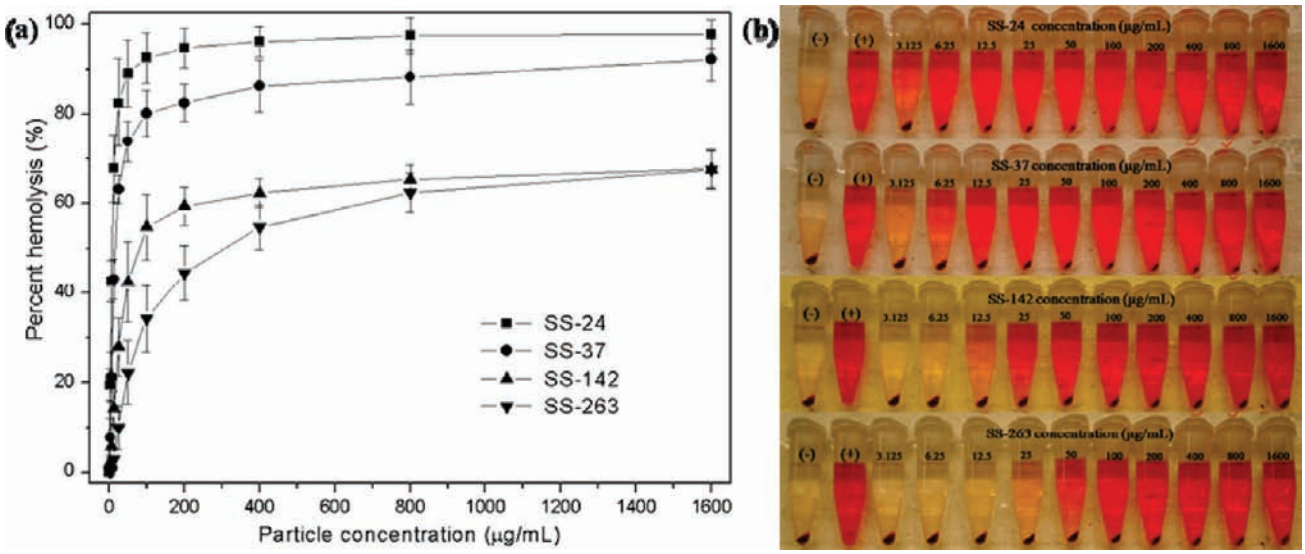


***Figure 4.*** (a) Percentage of hemolysis of RBCs incubated with four sizes of SS NPs at different concentrations ranging from 3.125 to 1600 $\mu$g/mL for 3 h. Data represent the mean ± SD from at least three independent experiments. (b) Photographs of hemolysis of RBCs in the presence of four sizes of SS NPs. The presence of red hemoglobin in the supernatant indicates damaged RBCs. D.I. water (+) and PBS (−) are used as positive and negative control, respectively.

**Table 2.** Surface Area of SS NPs and the Concentration of SS NPs Leading to a 50% Lysis of RBCs

| | SS-24 | SS-37 | SS-142 | SS-263 |
|---|---|---|---|---|
| $S_{BET}$ ($m^2$ $g^{-1}$) | 127 | 70 | 21 | 9 |
| $TC_{50}$[a] ($\mu$g/mL) | 8.8 | 18 | 94 | 307 |
| $TC_{50}$[a] (no. NPs/mL) | $5.5 \times 10^{11}$ | $3.1 \times 10^{11}$ | $2.8 \times 10^{10}$ | $1.5 \times 10^{10}$ |

[a] $TC_{50}$, expressed as $\mu$g and number of NPs per mL of solution.

4b. It is apparent that smaller SS NPs cause observable release of hemoglobin from damaged RBCs at lower nanoparticle exposure concentrations. This result demonstrates that the smaller particles have higher hemolytic activity than the larger particles. The concentration and number of SS NPs leading to 50% of lysis of RBCs for all SS NPs are listed in Table 2. Student's $t$ test analyses reveal significant differences among these $TC_{50}$ values for all samples ($p < 0.0001$). These data reveal a near-linear correlation between $TC_{50}$ and NP diameter (Figure S4, Supporting Information). The higher hemolytic activity of smaller SS NPs may be due to the larger surface area per gram, indicating higher number of silanol group present on the cell-contactable surface of the smaller SS NPs. The dose- and size-dependent cytotoxicity of nonporous amorphous silica NPs has been previously investigated using in vitro tetrazolium (methylthiazolyldiphenyltetrazolium bromide, MTT) and lactate dehydrogenase (LDH) assays in two recently published papers.[13,14] Napierska et al. and Yu et al. concluded that the cytotoxicity of the tested nanoparticles is strongly correlated to their size, because smaller particles have larger surface area per mass and show higher toxicity than larger particles. While it is true that toxicity mechanisms can be cell type-dependent, we have demonstrated herein that the simple hemolysis assay results are similar to those achieved with more complicated and expensive assays and thus will be a good first line assessment for candidate injectable nanoparticles.

Having demonstrated that the hemolytic activity accurately predicted the toxicity of nonporous silica, we turn to a systematic study of the hemolytic activity of MS NPs with varied sizes (Figure 5). As with the nonporous NPs, dose-dependent hemolysis behavior was also observed in all cases with MS NPs (Figure 5a). The size effect of MS NPs on hemolysis can be clearly seen when considering MS-42, MS-93, MS-155, and MS-225 NPs (Figure 5b). The $TC_{50}$'s for all MS NPs are listed in Table 3. With the exception of the MS-25 NP, the $TC_{50}$ values decrease as the diameter of MS NPs decreases (Figure S4 of the Supporting Information). The outlier characteristic of the MS-25 NP indicates that the size-dependent hemolytic activity holds only for MS NPs having a well-ordered mesoporous structure. Statistical comparisons showed significant differences between all samples ($p < 0.05$) except for the comparison between MS-25 and MS-155 ($p = 0.1756$), suggesting that the MS-25 and MS-155 have indistinguishable hemolytic activity. The MS-25 NP likely has lower than expected hemolytic activity due to the larger than expected pore size and greater primary pore volume (as shown in Table 1) compared to the larger

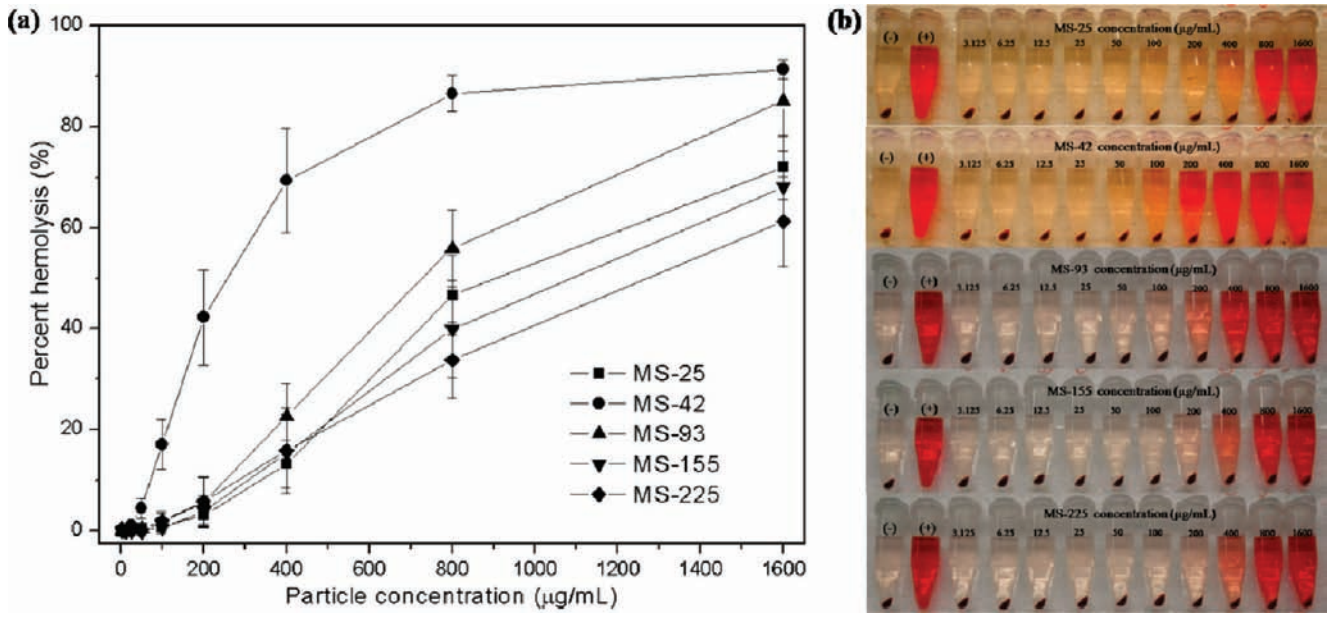


***Figure 5.*** (a) Percentage of hemolysis of RBCs in the presence of five sizes of MS NPs at different concentrations ranging from 3.125 to 1600 $\mu$g/mL for 3 h. Data represent the mean ± SD from at least three independent experiments. (b) Photographs of hemolysis of RBCs incubated with four sizes of MS NPs. The presence of red hemoglobin in the supernatant indicates damaged RBCs. D.I. water (+) and PBS (−) are used as positive and negative control, respectively.

***Table 3.*** Concentration of MS NPs Leading to a 50% Lysis of RBCs

| | MS-25 | MS-42 | MS-93 | MS-155 | MS-225 | MS-25 after 6-day aging | MS-42 after 6-day aging |
|---|---|---|---|---|---|---|---|
| $TC_{50}$[a] ($\mu$g/mL) | 991 | 282 | 765 | 1108 | 1295 | 124 | 34 |
| $TC_{50}$[a] (no. NPs/mL) | $1.8 \times 10^{14}$ | $7.3 \times 10^{12}$ | $1.9 \times 10^{12}$ | $6.1 \times 10^{11}$ | $5.8 \times 10^{10}$ | $2.1 \times 10^{13}$ | $8.8 \times 10^{11}$ |

[a] $TC_{50}$, expressed as $\mu$g and number of NPs per mL of solution.

diameter MS NPs, resulting in a smaller number of cell-contactable silanol groups on MS-25 NPs.

In short, compared to SS NPs with similar size, MS NPs show a reduction in hemolytic activity due to the voids on the surface of MS NPs. In addition, RBCs can tolerate more MS NPs than SS NPs with a similar size (as shown in Tables 1 and 2). Based on the hemolytic activity difference between the well-ordered and moderately ordered mesoporous NPs, it is clear that the pore structure of MS NPs, and thus the cell-contactable surface area, also influences the hemolytic activity of MS NPs.

**Effect of Mesopore Stability of MS NPs on Hemolysis.** To further explore the role of mesopore structure on silica nanoparticle toxicity, pore stability was examined among the various MS NPs. Pore stability is a concern because the surfactant template that originally supports the pore structure is removed before intravenous introduction, in part to allow introduction of a drug cargo and in part because the CTAB surfactant itself is highly cytotoxic. In the course of performing the aforementioned experiments, experimental observation revealed that there was an increase in the hemolytic activity of MS-25 and MS-42 NPs when the NPs were aged in PBS for 6 days (Figure 6a,b and S6, Supporting Information) before RBC incubation. The significant differences among $TC_{50}$ values (Table 3) between MS-25 and MS-25 after 6-day PBS aging and MS-42 and MS-42 after 6-day PBS aging were confirmed by student's *t* test ($p < 0.0001$). Three possible reasons were considered to explain this unintentional increase in apparent toxicity: residual surfactant, degradation product silicic acids, and pore collapse. The degradation of MS films and particles to monomeric and oligomeric silicic acids during aging in phosphate-buffered solutions or simulated body fluids has been reported in two recent papers.[20,31] Bass et al. revealed a dynamic change in the porous character of MS films under biological conditions and emphasized that this structural change would have significant implications on the use of these porous materials for drug delivery applications.[31] He et al. found that compromised structures produced degraded silicic acid products but that these species showed no toxicity to human breast cancer or African green monkey kidney cells.[20] While these two papers showed structural changes and examined the effects of any dissolved species, neither paper directly evaluates the impact of the altered mesoporous structure itself on cytotoxicity. To assess the three aforementioned possibilities, MS-25 and MS-42 NPs were suspended in PBS at the particle concentration of 2000 $\mu$g/mL, and after 6 days, the aged NPs were separated from the solution by centrifugation. Then, the hemolytic activity of supernatant was examined. Compared to a control CTAB-hemolysis experiment, no hemolysis was observed from the supernatant of MS-25 after 6-day PBS aging and MS-42 after 6-day PBS aging (Figure S7 of the Supporting Information). This implies that the amount of residual CTAB surfactant is less than 3.125 $\mu$g and not the source of increased hemolysis.

Because the hemolytic activity of MS NPs is strongly correlated to their porous structure and their cell-contactable surface area, XRD and $N_2$ adsorption−desorption measurements were applied to examine the pore integrity of aged MS NPs. The XRD data showed an intensity decrease in the (100) peak

(31) Bass, J. D.; Grosso, D.; Boissiere, C.; Belamie, E.; Coradin, T.; Sanchez, C. *Chem. Mater.* **2007**, *19*, 4349–4356.

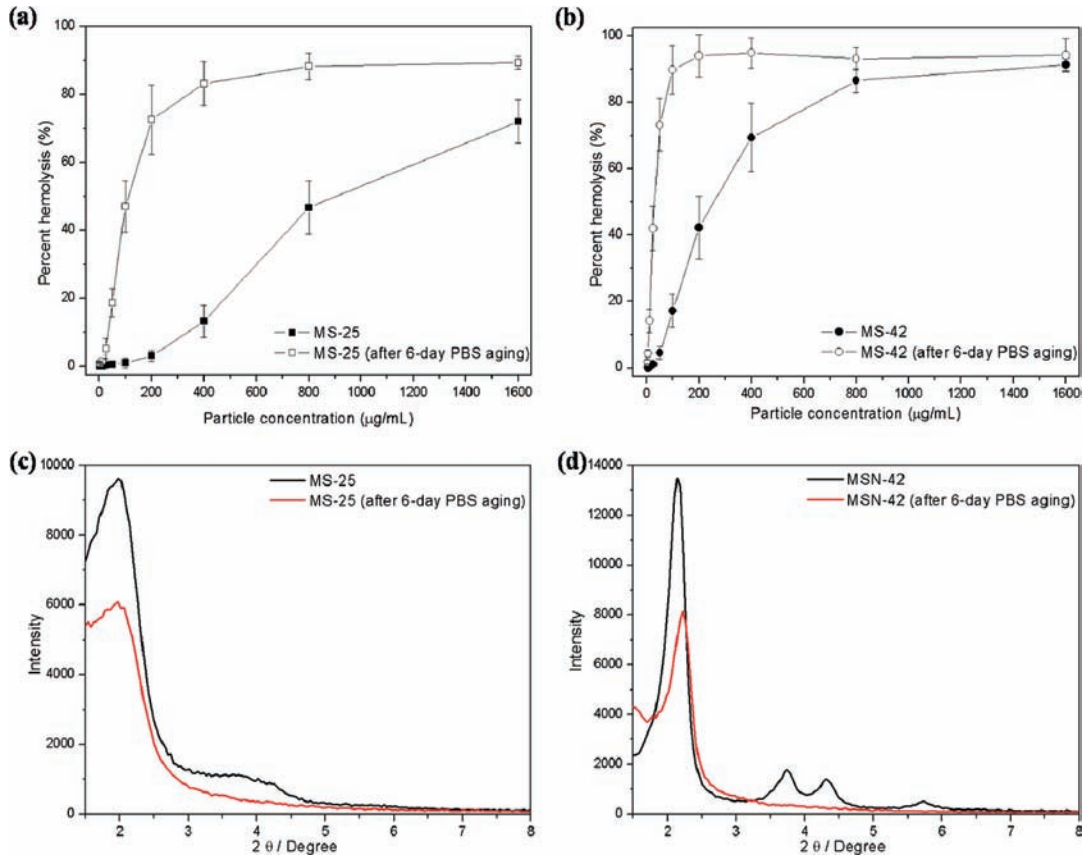


***Figure 6.*** Percentage of hemolysis of RBCs incubated with (a) MS-25 (square) and MS-25 after 6-day PBS aging (empty square); (b) MS-42 (circle) and MS-42 after 6-day PBS aging (empty circle). Low-angle XRD patterns of (c) MS-25 and MS-25 after 6-day PBS aging; (d) MS-42 and MS-42 after 6-day PBS aging.

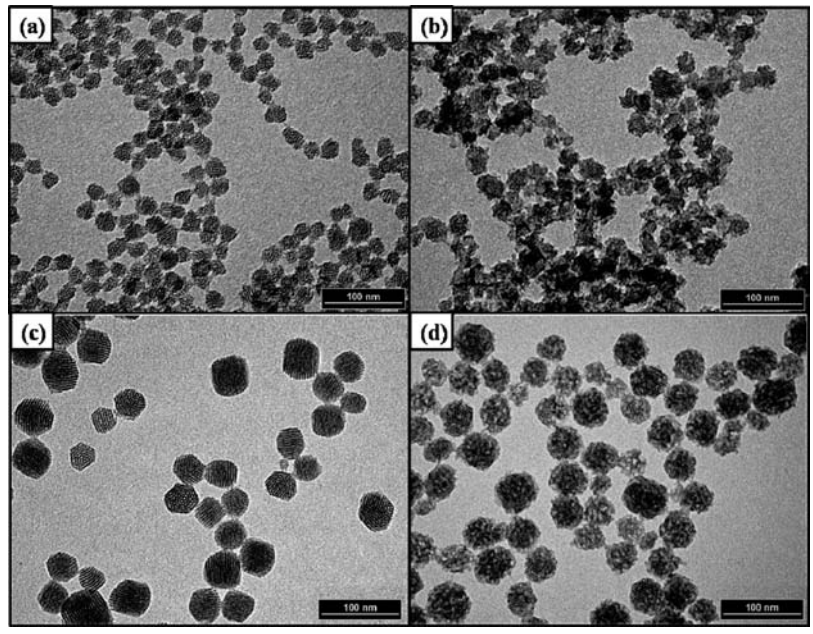


***Figure 7.*** TEM images of surfactant-free (a) MS-25 without PBS aging; (b) MS-25 after 6-day PBS aging; (c) MS-42 without PBS aging; and (d) MS-42 after 6-day PBS aging.

and disappearance of peaks at higher angles in both aged MS NP populations (Figure 6c,d). In addition, comparisons of TEM images between MS-25 and MS-42 without PBS aging and after 6-day PBS aging clearly showed that parts of the mesopores inside NPs collapsed after 6-day PBS aging (Figure 7). The disappearance of capillary adsorption in $N_2$ adsorption−desorption isotherms (Figure S8 of the Supporting Information) and the decrease in surface area and primary pore volume (as listed in Table 1) confirmed collapse of the mesopores inside NPs occurring during the PBS incubation. To further confirm the

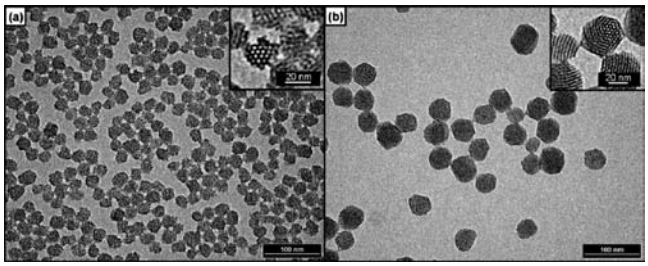

***Figure 8.*** TEM images of surfactant-free (a) MS-25@PEG and (b) MS-42@PEG. The inset is a high-magnification TEM showing 2D hexagonal mesopores inside MS-25@PEG and MS-42@PEG.

dissolution of MS NPs upon incubation in PBS and the subsequent pore collapse within the MS NPs, the quantity of silicic acid in solution after different PBS aging times was measured using the blue silicomolybdic assay.[32] The concentrations of degraded free silicon from MS-25 after 30-min aging, MS-42 NPs after 30-min aging, MS-25 after 6-day aging, and MS-42 after 6-day aging were 33, 37, 80, and 83 $\mu$g/mL respectively (Figure S9 of the Supporting Information). These results show that both MS-25 and MS-42 have similar dissolution rates during PBS incubation and that silica dissolution to silicic acid is fast and time-dependent. As previously discussed, the supernatant of the aged MS NPs was exposed to RBCs, and no detectable hemolysis was observed. These combined results demonstrate that the dissolved silicic acid species are not the source of increased hemolysis but that the liable feature must be a change in the nanoparticle surface itself. In fact, upon silica dissolution and pore collapse, the cell-contactable surface area is likely to increase, despite the total surface decrease, either by (1) elimination of void spaces or (2) lengthwise cracking of the pores to reveal the pore interior. To the best of our knowledge, none of the literature using mesoporous nanoparticles for drug delivery, imaging, and therapy has reported this pore collapse and its resultant effect on hemolytic activity. This work clearly demonstrates that the integrity of mesopores should be considered in future toxicological studies of MS NPs.

**Influence of PEG Surface Coating on Hemolytic Activity of MS NPs.** To counter the increase in hemolytic activity of MS NPs-collapsed mesopores, a surface modification strategy was employed. Based on the improved biocompatibility of MS NPs functionalized with a PEG coating reported in our previous work,[24] PEG-silane modified MS NPs were synthesized to compare the hemolytic activity with unfunctionalized MS NPs. As shown in Figure 8, the TEM images of surfactant-free MS-25@PEG and MS-42@PEG showed obvious porous structure within both NP populations. This result demonstrates that the PEG modification on the outer surface of MS NPs does not interrupt the ordering of mesopores. The mesopore stability in these modified NPs was examined after suspending PEG-coated MS NPs in PBS solutions for 6 days. The XRD patterns show evidence for some pore collapse after aging (Figure S10 of the Supporting Information). The hemolytic activity of the PEG-coated MS NPs and PEG-coated MS NPs after aging is shown in Figure 9a. Contrary to bare MS NPs, no hemolysis is apparent after 3 h blood incubation (Figure 9b and c), even at high nanoparticle doses (i.e., 1600 $\mu$g/mL) with collapsed mesopores. In addition, longer term biocompatibility of MS NPs was tested in the presence of MS-25@PEG after 6-day aging and MS-42@PEG after 6-day aging at the nanoparticle concentration of 1600 $\mu$g/mL. Neither of these aged NPs causes significant lysis of RBCs, even after 24 h incubation (Figure S11 of Supporting Information), revealing that PEG not only masks the surface silanol groups but also serves as a protecting layer, preventing the access of additional silanol groups from collapsed pores to RBCs. This simple surface modification strategy is critical to ensure the safety of MS NPs in biomedical applications.

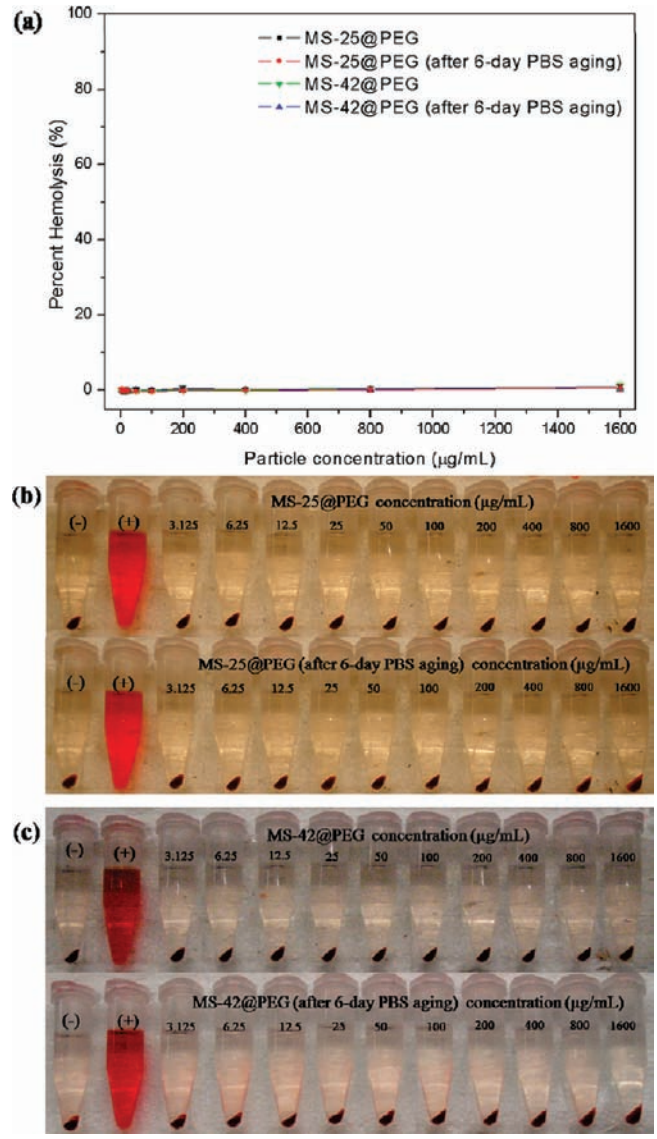


***Figure 9.*** (a) Percent hemolysis and (b, c) photographs of RBCs incubated with MS-25@PEG, MS-25@PEG after 6-day PBS aging, MS-42@PEG, and MS-42@PEG after 6-day PBS aging. Data represent the mean ± SD from at least three independent experiments.

## Conclusions

In summary, systematic comparisons of cytotoxicity of nonporous and porous silica NPs with varied sizes have been demonstrated using a simple hemolysis assay. All the nonporous and porous silica NPs show dose- and size-dependent hemolytic activity on RBCs, except for the case of the smallest MS NPs. Generally, smaller particles exhibited higher toxicity than larger particles as the $TC_{50}$ was expressed as mass concentration. MS NPs showed a reduction of hemolytic activity compared to similar sized nonporous counterparts. In addition to this size

(32) Coradin, T.; Eglin, D.; Livage, J. *Spectroscopy: Int. J.* **2004**, *18*, 567–576.

effect, the porous ordering structure and stability also influence hemolytic activity of MS NPs. Dissolution of silica and the subsequent collapse of pores inside the porous silica NPs after aging in PBS was confirmed by elemental analysis, XRD, $N_2$ adsorption−desorption isotherms, and TEM. The pore collapse leads to greatly increased hemolytic activity of mesoporous silica nanoparticles. However, it is possible to ameliorate the enhanced hemolytic activity of MS NPs via surface modification with a PEG-silane. While surface modification is a promising short-term solution to allow safe use of mesoporous silica nanoparticles, effort to maintain mesopore integrity will be an important subject of our future work.

**Acknowledgment.** This research was supported by a grant from the National Science Foundation (CHE-0645041). Y.-S. L. acknowledges support from a Taiwan Merit Scholarship (NSC-095-SAF-I-564-052-TMS) from National Science Council of Taiwan. All TEM and XRD measurements were carried out in the Institute of Technology Characterization Facility, University of Minnesota, which receives partial support from the NSF through the National Nanotechnology Infrastructure Network. We acknowledge Professor Michael Tsapatsis at the Department of Chemical Engineering and Materials Science, University of Minnesota, for assistance with nitrogen sorption measurements. We thank Özlem Ersin for assistance with handling human blood samples.

**Supporting Information Available:** Detailed synthesis conditions for four sizes of SS NPs and five sizes of MS NPs. Detailed calculations of number of SS and MS NPs per gram. Details of degraded free silicon quantification from MS-25 and MS-42 under different aging time. Size distributions of SS NPs with varied sizes. A photograph of five sizes of as-synthesized colloidal MS. $N_2$ adsorption−desorption isotherms of MS-25 and SS-24. Concentration-dependent hemolytic activity of MS NPs with varied sizes. Photographs of RBCs incubated with MS-25, MS-25 after 6-day PBS aging, MS-42, and MS-42 after 6-day PBS aging. Hemolysis and photographs of RBCs in the presence of CTAB and supernatant of MS-25 after 6-day PBS aging and MS-42 after 6-day PBS aging. Low-angle XRD of MS-25@PEG, MS-25@PEG after 6-day PBS aging, MS-42@PEG, and MS-42@PEG after 6-day PBS aging. Time-dependent hemolysis of RBCs incubated with MS-25@PEG after 6-day PBS aging and MS-42@PEG after 6-day PBS aging. This material is available free of charge via the Internet at http://pubs.acs.org.

JA910846Q